# Occurrence, characterisation and fate of (nano)particulate Ti and Ag in two Norwegian wastewater treatment plants

Fabio Polesel[1†*], Julia Farkas[2†], Marianne Kjos[3], Patricia Almeida Carvalho[3], Xavier Flores-Alsina[4], Krist V. Gernaey[4], Steffen Foss Hansen[1], Benedek Gy. Plósz[1,5], Andy M. Booth[2*]

[1]DTU Environment, Technical University of Denmark, Bygningstorvet, Building 115, 2800 Kongens Lyngby, Denmark

[2]SINTEF Ocean, Brattørkaia 17C, 7010 Trondheim, Norway

[3]SINTEF Materials and Chemistry, Postboks 4760 Torgarden, 7465 Trondheim, Norway

[4]Process and Systems Engineering Center (PROSYS), Department of Chemical and Biochemical Engineering, Technical University of Denmark, Søltofts Plads, Building 229, 2800 Kongens Lyngby, Denmark

[5]Department of Chemical Engineering, University of Bath, Claverton Down, Bath BA2 7AY, UK

[†]The authors equally contributed to the study.

*Corresponding authors: andy.booth@sintef.no; fabp@env.dtu.dk

**Abstract**

Due to their widespread application in consumer products, elemental titanium (e.g., titanium dioxide, $TiO_2$) and silver (Ag), also in nanoparticulate form, are increasingly released from households and industrial facilities to urban wastewater treatment plants (WWTPs). A seven-day sampling campaign was conducted in two full-scale WWTPs in Trondheim (Norway) employing only primary treatment. We assessed the occurrence and elimination of Ti and Ag, and conducted size-based fractionation using sequential filtration of influent samples to separate particulate, colloidal and dissolved fractions. Eight-hour composite influent samples were collected to assess diurnal variations in total Ti and Ag influx. Measured influent Ti concentrations (up to 290 µg $L^{-1}$) were significantly higher than Ag (<0.15–2.1 µg $L^{-1}$), being mostly associated with suspended solids (>0.7 µm). Removal efficiencies ≥70% were observed for both elements, requiring for one WWTP to account for the high Ti content (~2 g $L^{-1}$) in the flocculant. Nano- and micron-sized Ti particles were observed with scanning transmission electron microscopy (STEM) in influent, effluent and biosolids, while Ag nanoparticles were detected in biosolids only. Diurnal profiles of influent Ti were correlated to flow and pollutant concentration patterns (especially total suspended solids), with peaks during the morning and/or evening and minima at night, indicating household discharges as predominant source. Irregular profiles were exhibited by influent Ag, with periodic concentration spikes suggesting short-term discharges from one or few point sources (e.g., industry). Influent Ti and Ag dynamics were reproduced using a disturbance scenario generator model, and we estimated per capita loads of Ti (42–45 mg $cap^{-1}$ $d^{-1}$) and Ag (0.11 mg $cap^{-1}$ $d^{-1}$) from households as well as additional Ag load (14–22 g $d^{-1}$) from point discharge. This is the first study to experimentally and mathematically describe short-term release dynamics and dry-weather sources of emissions of Ti and Ag in municipal WWTPs and receiving environments.

**Keywords:** nanoparticles, titanium dioxide, silver, wastewater, diurnal variation, modelling

## 1. Introduction

The release of metals to sewer systems and wastewater treatment plants (WWTPs) has been traditionally linked to industrial discharges (Shafer et al. 1998). Stormwater runoff (containing metals originating from traffic, atmospheric deposition and catchment surfaces) can also contribute to such emissions under wet weather conditions (Becouze-Lareure et al. 2016, Sabin et al. 2005). In the past decade, increasing dry weather discharges from households have been associated with the presence of metals in consumer products, also in the form of pigment-sized particles and metallic nanoparticles (NPs). Titanium (Ti) and silver (Ag) NPs have frequently been detected in WWTP influents (Kiser et al. 2009, Li et al. 2013), owing to their widespread application in clothing (Benn and Westerhoff 2008, Mitrano et al. 2016), washing equipment (Farkas et al. 2011), personal care and hygiene products (Benn and Westerhoff 2008, Contado and Pagnoni 2008, Mackevica et al. 2017, Weir et al. 2012) and food (Weir et al. 2012, Peters et al. 2014).

Attempts have been made to characterize metal fractions in wastewater through size-based fractionation (Kiser et al. 2009, Johnson et al. 2014). Although these studies only assessed either Ti or Ag, they describe a relevant approach for the quantification of metal fractions in particulate, colloidal and dissolved forms. Electron microscopy has proven reliable for identification of Ti and Ag NPs within the different fractions (Kiser et al. 2009, Kaegi et al. 2013). High removal efficiencies (>90%) have been reported in pilot- and full-scale WWTPs for (nano)metallic Ti and Ag (Shafer et al. 1998, Kiser et al. 2009, Li et al. 2013, Johnson et al. 2014, Kaegi et al. 2011, Östman et al. 2017, Westerhoff et al. 2011). This results from sorption to solids and incorporation in primary and secondary sludge, with potential discharge of (nano)metals to soils following agricultural reuse of biosolids as fertilizer. While these

70 studies have investigated the fate and removal in WWTPs with biological treatment, limited
71 information exists for facilities employing only preliminary and primary physico-chemical
72 treatment. These facilities are the most common in Norway, and are known to exhibit reduced
73 removal of conventional pollutants (e.g. solids, organic matter, nutrients) and organic
74 micropollutants (Vogelsang et al. 2006).
75
76 Temporal trends in the dry weather occurrence of Ti and Ag in WWTP influents (diurnal,
77 intra-day, seasonal variations) are largely unknown, likely depending on the type and
78 characteristics of the served catchment. Composite sampling in influents at higher than daily
79 resolution (2-h to 8-h composites) has been previously used to study diurnal release patterns of
80 pharmaceuticals (Plósz et al. 2010) and illicit drugs (Ramin 2016) and to identify point sources
81 of biocide emissions (Bollmann et al. 2014). In situations where removal is incomplete,
82 influent pollutant loads can quickly propagate to effluents, especially in WWTPs with short
83 residence times. Elucidating temporal trends of Ti and Ag in influents can be beneficial for (i)
84 identifying their predominant uses and sources of discharge; (ii) forecasting emission
85 dynamics from WWTPs; and (iii) developing pollutant attenuation strategies by WWTP
86 operators. In this context, influent generator algorithms (Ort et al. 2005; De Keyser et al.,
87 2010; Gernaey et al. 2011) offer a useful tool to extrapolate short-to-medium-term (diurnal to
88 seasonal) dynamics, complementing existing mass flux analysis tools relying (especially for
89 manufactured NPs) on steady-state (Gottschalk et al. 2009) or dynamic predictions at multi-
90 year scale (Sun et al. 2016).
91
92 The objective of the current study was to assess the occurrence and fate of Ti and Ag in two
93 Norwegian WWTPs employing primary sewage treatment. We have (i) evaluated diurnal and

intra-day variations in Ti and Ag loads; (ii) developed and tested a method to characterize Ti and Ag as particulate (i.e. associated to suspended solids), colloidal and dissolved fractions; and (iii) identified the presence and the size of Ti and Ag NPs by electron microscopy. In addition, an influent disturbance scenario generator has been adapted to the two WWTP catchments under study, and used to predict occurrence dynamics of influent Ti and Ag and to estimate per capita loads and loads from point sources, based on measured time series. Finally, the fate of Ti and Ag in the two WWTPs was assessed by measuring residual Ti and Ag in final effluents and treated sludge, allowing for the quantification of removal efficiencies during primary wastewater treatment and release to receiving environments.

## 2. Materials and methods

### *2.1. Wastewater treatment plants*

The city of Trondheim, Norway is served by two main WWTPs (Fig. 1a). Ladehammeren (LARA) and Høvringen (HØRA) have a design capacity of 120,000 PE and 170,000 PE, respectively, with substantial industrial loading contributions (up to 40% for LARA). The wastewater treatment train in LARA and HØRA (Fig. 1b) includes fine screening, sand and fat removal, chemically-aided flocculation-coagulation ($ClFeO_4S$ and polyamine in LARA, polyacrylamide in HØRA) and primary sedimentation (with longitudinal-flow basins in LARA and vertical-flow basins in HØRA). The effluents from each WWTP are discharged into Trondheimsfjord at depths between 40 and 65 m. In both WWTPs, primary sludge is thickened and pasteurized before anaerobic digestion (mesophilic, residence time=15 d), with eventual dewatering through centrifugation (Fig. 1b).

**< Figure 1 >**

### *2.2. Sampling*

A seven-day sampling campaign (October 2016) was conducted in parallel in the two WWTPs during a dry weather period. Samples were collected on 6–8$^{th}$ October (Thursday to Saturday) and 10–15$^{th}$ October (Monday to Saturday; for details see Table S1). To determine the total influx and removal efficiencies of Ti and Ag, 24-h composite samples of untreated influent, final effluent and sludge samples were collected (Fig. 1b). To ensure complete mass balancing, effluent samples were collected after vigorous shaking of the sampling container, thus ensuring representative and homogeneous solid content, and analysed without prior removal of suspended solids (e.g., via filtration).

Furthermore, 8-h flow-proportional samples of raw influent wastewater were collected to identify potential diurnal influx patterns of Ti and Ag, as well as conventional pollutants. To avoid sample contamination, sampling containers and equipment used for sample treatment and storage (except for metal free centrifuge tubes) were subjected to a multiple step cleaning procedure before each use: surfactant wash, rinse with distilled water, soak in ultrapure $HNO_3$ (10%) for at least 3 h and rinse with distilled water.

#### *2.2.1. Influx and removal efficiency of Ti and Ag*

To determine the incoming loads and the removal efficiency of Ti and Ag in the WWTPs, daily composite samples (LARA: $n$=6; HØRA: $n$=5) were collected. The 24-h volume-proportional ($\Delta V$=152 m$^3$ in LARA, 264 m$^3$ in HØRA) composite samples of the untreated influent (LARA-IN) and the final effluent (LARA-OUT, HØRA-OUT) were collected using refrigerated automatic samplers. Due to limitations in sampling logistics, 24-h flow-proportional composite samples for HØRA-IN were derived by compositing 8-h flow-proportional samples (see 2.2.2).

To account for the hydraulic residence time in the two WWTPs, effluent sample collection was conducted with a delay relative to the influent sampling. Grab samples of biosolids (LARA: $n$=3; HØRA: $n$=2) were collected at the end of the sludge treatment line (Fig. 1b). Biosolids samples were stored at -20°C until analysis.

*2.2.2. Diurnal influx patterns of Ti and Ag and conventional pollutants*

To determine influx patterns and diurnal loading variations of Ti, Ag and conventional pollutants (organic matter, suspended solids, nitrogen, phosphorus) in the WWTP influents, intra-day monitoring was conducted. One-hour time-proportional composite samples (frequency=5 min) were collected each day in clean polyethylene bottles (stored with ice and cooling elements) using portable automatic samplers (Teledyne ISCO®, Lincoln NE, US). At the end of the 24-h interval, 1-h samples were collected and immediately combined flow-proportionally into 8-h samples. Flow-proportional compositing was based on real-time influent flow data collected from the two WWTPs, comparable to previous studies (Plósz et al. 2010, Lai et al. 2013, Ramin 2016). The 8-h intervals were selected to cover morning (M), evening (E) and night (N) discharges, based on preliminary assessment of typical flow pattern data and considerations on the catchment size. Samples were processed within 1 h of compositing.

## *2.3. Sample preparation and analytical methods*

*2.3.1. Sample concentration*

To achieve quantifiable concentrations of Ti and Ag in IN and OUT 24-h composite samples, 40 mL of each sample was concentrated by evaporation immediately after collection. The samples were evaporated to dryness in cleaned glass vials in a water bath (90–95°C) and stored

166 at 4°C prior to analysis by inductively coupled plasma mass spectrometry (ICP-MS). To
167 determine potential background contamination, 40 mL of Milli-Q water (Merck Millipore,
168 USA) (*n*=3) was evaporated simultaneously with the wastewater samples.
169
170 *2.3.2. Size-based fractionation of Ti and Ag in raw WWTP influent*
171 To determine the occurrence of Ti and Ag in different fractions in the untreated influent
172 wastewater, a size-based fractionation of the pooled 8 h samples (M, E, N) was performed as
173 described in Fig. 2. A detailed description of the approach is provided in the Supporting
174 Information. Briefly, samples (85–100 mL) were sequentially filtered through 2.7 µm and 0.7
175 µm pore size glass fibre filters. The dissolved (ionic) fraction was isolated from the colloidal
176 fraction (0.7 µm filtrate) using ultrafiltration (3 kDa). Ti and Ag were quantified for the 2.7
177 and 0.7 µm filters (particulate fraction), the 0.7 µm filtrate (colloidal and dissolved fraction)
178 and 3 kDa filtrate (dissolved fraction) by ICP-MS (Fig. 2). Total amounts of Ti and Ag in each
179 8-h composite sample were calculated as the sum of the three fractions.
180 **< Figure 2 >**
181
182 *2.3.3. Conventional pollutants analysis*
183 Influent samples (8-h composites) were analysed for conventional pollutants, including total
184 chemical oxygen demand ($COD_{tot}$), soluble COD ($COD_{sol}$), total nitrogen ($N_{tot}$), ammonium
185 nitrogen ($NH_4$-N), total phosphorus ($P_{tot}$) and TSS. Dissolved analytes were quantified in the
186 0.7 µm filtrate. Non-filtered and filtered samples were stored in plastic vials and frozen until
187 analysis. $COD_{tot}$, $COD_{sol}$, $N_{tot}$ and $P_{tot}$ concentrations were quantified using Hach-Lange®
188 colorimetric kits (LCK314, LCK514, LCK338 and LCK348) and a Hach-Lange® DR 2800
189 spectrophotometer. NH4-N concentrations were quantified using Merck® colorimetric kits

(100683) and Merck® Spectroquant® spectrophotometer. Total suspended solids (TSS) were quantified by combining the solid content from the 2.7 µm and 0.7 µm filters.

*2.3.4. Ti and Ag quantification*

Ti and Ag were quantified in 24–h composite samples (IN and OUT), biosolids, and in each size fraction of the 8-h influent samples using ICP-MS. Samples of the inorganic flocculant ($ClFeO_4S$) were also analysed for Ti content. For Ag analysis, filters were digested with 8 mL (2.7 µm) or 5 mL (0.7 µm) of 65% $HNO_3$ in an ultrasonic bath (80°C, 2 h), centrifuged and diluted with ultrapure water (MilliQ). The remaining solution was then supplemented with 8 mL (2.7 µm) or 5 mL (0.7 µm) ultrapure water and 1 mL 47–51% hydrofluoric acid (HF), digested for 2 h, centrifuged and diluted with MilliQ water prior to Ti analysis. The 0.7 µm filtrate was diluted (1:1) with 10% $HNO_3$ and analysed for both Ti and Ag. The 3 kDa filtrate was analysed for Ti and Ag without pre-treatment.

Evaporated samples were dissolved in 5% $HNO_3$ overnight. Subsequently, 5 mL of concentrated $HNO_3$ were added and the samples digested in an ultrasonic bath for 2 h at 80°C. Aliquots were collected for Ag quantification, centrifuged and diluted prior to analysis. For Ti quantification, 2 mL of the digested solution was treated with 200 µL HF, digested for 2 h, diluted and analyzed. Biosolids samples were first digested with $HNO_3$ in an ultrasonic bath (80°C, 2 h) before HF was added and additional digestion (2 h) was carried out. Samples were analyzed with inductively coupled plasma triple quadrupole mass spectrometry (ICPQQQ, Agilent 8800; Agilent Technologies, USA) equipped with a SPS4 autosampler. Samples were quantified using internal standards $^{115}In$ and $^{89}Y$ (Inorganic Ventures, USA).

214

215 *2.3.5. Electron microscopy*

216 Scanning transmission electron microscopy (STEM) coupled with energy-dispersive X-ray
217 spectroscopy (EDS) was used to (i) identify Ti and Ag potentially present as nano-particulates
218 in the total samples and size fractions of wastewater influent, (ii) to characterise Ti and Ag
219 particles (size and shape) and (iii) to study their association with other particulate matter. A
220 detailed summary of the sample preparation procedures is presented in the SI. Briefly,
221 unfiltered and filtered samples (~10 µL) were applied onto TEM grids (copper grids with a
222 lacey carbon film, mesh size 200; Agar Scientific, UK). STEM imaging was performed using
223 an FEI Titan G2 60-300 microscope equipped with a DCOR probe Cs-aberration corrector
224 operating at 300 kV. EDS was conducted with a Bruker SUPERX detector coupled to the same
225 instrument.

226

227 ***2.4 Statistical analysis***

228 Comparative data analyses of Ti and Ag influent concentrations were performed with
229 GraphPad Prism 7 (GraphPad Software Inc., USA). The data sets were analysed for normality
230 (Shapiro-Wilk normality test). To detect significant differences between treatments, data were
231 analysed either with ANOVA followed by Tukey's multiple comparisons test or with the non-
232 parametric Kruskal-Wallis statistics followed by Dunn's test, with significance levels set for
233 $p<0.05$. Correlations between 8-h influent concentrations of Ti, Ag and of conventional
234 pollutants ($COD_{tot}$, $COD_{sol}$, $N_{tot}$, $NH_4$-N and $P_{tot}$) were determined using SigmaPlot 11.0
235 (Systat Inc., Germany) to explore possible diurnal co-occurrence patterns.

236

### *2.5 Modelling dynamics of influent flow rate and concentrations of traditional pollutants, Ti and Ag*

Based on 8-h measurements during the sampling campaign, dynamics in the occurrence of Ti and Ag were simulated using a phenomenological influent disturbance scenario generator (Gernaey et al., 2011). This modelling algorithm allows for the generation of high-frequency time series of flow rate and pollutant concentrations in a WWTP influent based on (i) the characteristics (e.g. population, area) of the upstream catchment; and (ii) (dynamic) flow and pollutant load contribution from households, industries, groundwater infiltration and (if relevant) rainfall. A description of the model is provided in the Supporting Information. As compared to previous studies (Snip et al. 2016, Flores-Alsina et al. 2014), a simplified step-by-step calibration procedure was used to fit simulated time series to monitoring results, and to generate consistent concentration profiles for Ti and Ag:

(i) Flow rate predictions were calibrated to high-frequency (5 min for LARA, 2 min for HØRA) measurements using existing knowledge (residential population: 60,000 and 120,000 inhabitants in LARA and HØRA catchments, respectively; groundwater infiltration) and by manually adjusting the flow rate per capita ($Q_{PE}$, L $cap^{-1}$ $d^{-1}$), the average industrial flow rate ($Q_{ind}$, $m^3$ $d^{-1}$) and the sewer length (parameter *subarea*).

(ii) Conventional pollutant concentration profiles (8-h samples) were calibrated by manually adjusting household per capita load (g $cap^{-1}$ $d^{-1}$), based on typical values, and load contributions from industries, in agreement with the type of industries operating in the catchments. In both flow rate (i) and traditional pollutants (ii) model blocks, default diurnal profiles were used. Nevertheless, hourly multiplying factors were adjusted to match intra-day patterns where necessary.

(iii) Correlations between influent concentrations of Ti, Ag and of conventional pollutant indicators (TSS, $COD_{tot}$, $COD_{sol}$, $N_{tot}$, $NH_4$-N, $P_{tot}$) were explored. Ti and Ag profiles were generated based on previously established correlations, i.e. using the slope of the correlation as conversion factor, and compared with measured concentration profiles. Per capita loads of Ti and Ag and, if relevant, loads from point sources were estimated.

Correspondence between model simulations and measurements in (i), (ii) and (iii) was verified by considering the coefficient of determination ($R^2$) and root mean square error (RMSE) as objective functions. Detailed information about the model structure and parameter values used in this study is presented in the Supporting Information.

## 3. Results

### *3.1. Occurrence and removal of Ti and Ag*

Ti concentrations determined in 24-h composite samples of influent wastewater ranged from 120 µg $L^{-1}$ to 236 µg $L^{-1}$, and were slightly, but not significantly lower in LARA (154 ± 34 µg $L^{-1}$) than in HØRA (188 ± 44 µg $L^{-1}$) (Fig. 3, Table S3). Mean Ti concentrations in the final effluent were 92.8 ± 5.8 µg $L^{-1}$ in LARA and 28.2 ± 4.3 µg $L^{-1}$ in HØRA, while concentrations in biosolids were 1011 ± 59 mg $kg^{-1}$ in LARA and 593 ± 17 mg $kg^{-1}$ in HØRA (Table S3). Removal efficiencies, calculated by comparing influent and effluent Ti concentrations, were 37% ± 13% in LARA and 84% ± 4% in HØRA (Fig. 3). Consistently low removal efficiencies in LARA may be explained by the use of $ClFeO_4S$ as an inorganic flocculant, which was found to contain approximately 1.9 g $L^{-1}$ (1.25 g $kg^{-1}$) of Ti. When considering the influent Ti load with the flocculant, the removal efficiency in LARA (81%) was in agreement with HØRA (Fig. 3).

Ag concentrations in influent wastewater were approximately three orders of magnitude lower than for Ti. Average Ag concentrations in 24-h composite samples were 0.19 ± 0.02 µg $L^{-1}$ in LARA, while being significantly higher in HØRA (0.59 ± 0.57 µg $L^{-1}$; $p<0.05$). The large variation of influent Ag concentrations in HØRA was associated with significant intra-day variation, which was also observed in 8-h measurements. These differences were also reflected in effluent concentrations, which were 0.04 ± 0.01 µg $L^{-1}$ in LARA and 0.24 ± 0.37 µg $L^{-1}$ in HØRA. Treated biosolids were found to contain 0.41 ± 0.04 mg $kg^{-1}$ in LARA and 1.10 ± 0.09 mg $kg^{-1}$ in HØRA. Calculated removal efficiencies for Ag were comparable in the two WWTPs, being 78 ± 4% in LARA and 69 ± 16% in HØRA.

**< Figure 3 >**

### *3.2. Ti and Ag in WWTP influent*

#### *3.2.1. Diurnal variations*

The selection of 8-h intervals to assess diurnal variations in Ti and Ag occurrence permitted a comparable and consistent subdivision of the daily influent flow rate at the two WWTPs between morning (M), evening (E) and night (N) discharges. Fractions of daily influent flow rate in M (LARA: 37.5% ± 2.5%; HØRA: 37.6% ± 0.7%), E (LARA: 38.2% ± 1.8%; HØRA: 37.4% ± 0.4%) and N (LARA: 24.3% ± 0.9%; HØRA: 25.0% ± 0.6%) periods accordingly exhibited small intra-day variability and were similar in the two WWTPs, with significantly lower flow in night periods ($p<0.05$).

Figure 4 shows the diurnal profiles of total Ti and Ag concentrations in influents over seven days. Comparable Ti concentrations were quantified in 8-h samples from LARA (66–281 µg $L^{-}$

[1]) and HØRA (92–290 µg $L^{-1}$), and no significant difference was observed when comparing the two WWTPs for each 8-h interval (Fig. 4a). Ti concentrations followed typical diurnal trends of influent flow rate and pollutant concentrations in municipal WWTP influents (M and/or E peaks, N minima). Accordingly, Ti concentrations in M and E samples were significantly higher than in N samples for both LARA and HØRA ($p<0.05$). Overall, Ti concentrations exhibited rather good correlation ($R^2=0.76$) with TSS in both WWTPs (Fig. 4b). The slope of the correlation was comparable in the two WWTPs, indicating similar amounts of Ti per mg of TSS present in the influent (0.49 µgTi/mgTSS in LARA, 0.47 µgTi/mgTSS in HØRA). Relevant correlations with other conventional pollutant indicators are presented in the Supporting Information. Ti concentrations were found to correlate well with influent $COD_{tot}$ (Fig. S9b, S10b), with $R^2=0.90$ in HØRA.

Ag concentrations (Fig. 4c) were considerably lower than Ti concentrations in both WWTPs (<0.15–2.1 µg $L^{-1}$). Ag concentrations at LARA remained relatively constant, whilst an irregular Ag release pattern was observed at HØRA, with considerable variation in E periods. Ag concentrations were significantly higher ($p<0.05$) in E samples from HØRA compared to LARA, whilst HØRA E was significantly higher than HØRA N ($p<0.05$). For LARA, no relevant correlation could be found between influent Ag and conventional pollutant concentrations ($R^2<0.20$). In both Thursday-to-Friday E samples from HØRA, increased Ag concentrations (>1.5 µg $L^{-1}$, on average four times higher than the other measurements) were detected (Fig. 4c–d, Fig. 9e). In the first sampling day, this was accompanied by a considerable increase of Ag effluent concentrations (Fig. S2). When excluding peak values, Ag concentrations in HØRA exhibited a rather good correlation with $P_{tot}$ ($R^2=0.62$, Fig. 4d). In

contrast to Ti, weaker correlations were observed between Ag and TSS or $COD_{tot}$ (Fig. S10d–e).

**< Figure 4 >**

*3.2.2. Fractionation and characterization*

The size-based fractionation assessment indicated that most of the influent Ti and Ag occurred in the particulate phase (>0.7 µm), being either in particulate form or associated with wastewater solids (Fig. 5). More than 99% of the influent Ti and >95% of the influent Ag was present in the particulate fraction in both WWTPs (Fig. 5). In LARA, 92% of Ti occurred in the >2.7 µm fraction, with approximately 8% found in the 0.7–2.7 µm fraction. In HØRA, 95% of the Ti was detected in the >2.7 fraction, with ~5% in the 0.7–2.7 µm fraction. These results correlate well with TSS concentrations, for which the 0.7–2.7 µm size fraction represented 8% and 5% of the total concentration in LARA and HØRA, respectively. Approximately 3–5% of Ag occurred in the colloidal and ionic fractions, whilst Ti (≤0.2%) was negligible in these two fractions (Fig. 5). It was not possible to separately quantify colloidal and ionic Ti and Ag, which were therefore combined in the <0.7 µm fraction.

STEM of influent wastewater samples revealed that elemental Ti and titanium dioxide ($TiO_2$) were frequently present as particles associated with solids (Fig. 6a–b, Fig. S4). Individual particle diameters ranged from approximately 50 nm to 500 nm, while agglomerates and aggregates reached >500 µm (Fig. 6 b–d; Fig. S3–S4). Furthermore, Ti particles were frequently detected in biosolids, mostly in association with Fe (Fig. 7a). Ti particles were also detected with STEM in effluent samples (Fig. S6), showing their potential release into the receiving environment. Nanoparticulate Ag could not be detected with STEM in influent and

355 effluent samples, possibly due to low concentrations. However, Ag NPs were detected in
356 treated biosolids samples (Fig. 7b).

357 **< Figure 6 >**

358 **< Figure 7 >**

359

360 *3.2.3. Modelling influent Ti and Ag dynamics*

361 The influent flow generator module was calibrated against high-frequency measurements in
362 both HØRA and LARA (Fig. 8a, 9a). A comparably good fit ($R^2$=0.52–0.79; RMSE=4358–
363 5232 $m^3$ $d^{-1}$) was achieved by (i) setting per capita residential discharge ($Q_{PE}$) to 170 L $cap^{-1}$ $d^{-1}$
364 in both catchments (LARA: 60,000 inhabitants; HØRA: 120,000 inhabitants), and (ii)
365 adjusting the parameter *subarea* (4 for LARA, 8 for HØRA), which determines the in-sewer
366 residence time and dispersion, in agreement with the surface area of the two catchments (Fig.
367 1). For HØRA, higher contribution of infiltration (+43%) had to be assumed in the first two
368 days of the sampling campaign due to rainfall in the previous days, resulting in increased flow
369 rate (Fig. 9a) and simultaneous dilution of all influent pollutant concentrations (Fig. S8).

370

371 Given that TSS and $P_{tot}$ exhibited the best correlation with Ti and Ag ($R^2$=0.62–0.76),
372 respectively, concentration profiles of these traditional pollutant indicators were first calibrated
373 (Fig. 8b, 9b–c). TSS was selected over $COD_{tot}$ as it provided a better indication of Ti
374 occurrence in both WWTPs, and in consideration of the similarity in Ti content per amount of
375 TSS. Simulated TSS patterns ($R^2$=0.75–0.88; RMSE=42.8–62.5 mg $L^{-1}$) were obtained with
376 similar per capita loads $TSS_{PE}$ = 86 and 95 gTSS $cap^{-1}$ $d^{-1}$ in LARA and HØRA, respectively.
377 Industrial load contribution was set to 14% in LARA and 30% in HØRA, hence justifying
378 higher influent TSS concentrations in HØRA. These numbers reflect the substantial load

contribution of food and beverage industry in LARA. Diurnal release patterns of TSS were adjusted by fitting simulations to 1-h concentration profiles, derived from hourly composite samples (Fig. S11). For HØRA, the simulated $P_{tot}$ pattern ($R^2$=0.69; RMSE=0.9 mg $L^{-1}$) was obtained with household load $P_{tot,PE}$ = 1.7 gP $cap^{-1}$ $d^{-1}$.

Ti concentration profiles in both WWTPs were predicted from TSS profiles by using the respective average Ti content in TSS, as given in Figure 4b. Simulated time series (Figures 8c, 9d) were generally in agreement with measured profiles ($R^2$=0.57–0.62; RMSE=41.4–41.6 µg $L^{-1}$). Accordingly, per capita loads of Ti from household discharges were estimated to be 42.2 mg $cap^{-1}$ $d^{-1}$ for LARA and 44.6 mg $cap^{-1}$ $d^{-1}$ for HØRA.

A simulated profile of the background Ag concentration in HØRA influent was obtained from the calibrated $P_{tot}$ profile (dotted line, Fig. 9e). This profile described the occurrence of Ag due to baseline activities in the catchment, corresponding to a per capita discharge of 0.11 mg $cap^{-1}$ $d^{-1}$ in HØRA. As expected, this profile did not adequately capture the systematic increase of Ag concentration registered during the sampling campaign, which was therefore attributed to discharge from a point source (e.g., industry). It is thus proposed that a pulse discharge of Ag occurred on Thursday evenings, with the significant increase of influent Ag concentration corresponding to an additional load of 14–22 g $d^{-1}$ from a single point source.

**< Figure 8 >**

**< Figure 9 >**

## 4. Discussion

### *4.1. Influx, removal and release of Ti*

Ti concentrations in untreated influent determined in this study (154 ± 34 µg $L^{-1}$ in LARA, 188 ± 44 µg $L^{-1}$ in HØRA) are in agreement with other studies, which reported mean Ti concentrations of 185–377 µg $L^{-1}$ in WWTP influents in Arizona (Kiser et al. 2009, Westerhoff et al. 2011).

Despite employing similar primary treatment (comprising both mechanical and chemical steps), calculated Ti removal in LARA was significantly lower (37 ± 12%) than for HØRA (84% ± 4%). This is due to the application of $ClFeO_4S$ flocculant in LARA, which was found to contain ~2 g $L^{-1}$ Ti. When considering influent Ti loading with untreated wastewater and flocculant, the removal efficiency was estimated to be 81% for LARA, similarly to what observed in HØRA. This further explains the 2-fold increase of Ti concentrations in biosolids in LARA (1010 µg $g^{-1}$) compared to HØRA (593 µg $g^{-1}$), despite the lower Ti influent values (Fig. 3). For the first time, this study has shown that inorganic flocculants represent a significant source of Ti in WWTPs. Future studies should therefore consider all the potential influent streams when performing mass balances and calculating removal efficiencies of Ti.

A comparison with previous investigations revealed that measured Ti removal efficiencies in HØRA (on average 84%) were lower than observations in other WWTPs with secondary and tertiary treatment, where Ti removal efficiencies are typically >90% (Kiser et al. 2009, Westerhoff et al. 2011). HØRA typically achieves TSS removal efficiencies of 75% (data not shown), well below the performance of WWTPs employing secondary treatment. Therefore, incomplete Ti removal in HØRA (when compared to secondary/tertiary WWTPs) can be attributed to the presence of primary treatment only. Furthermore, differences may be attributed to the fact that earlier removal efficiency determinations were made using grab

425 sampling of influent and effluent, i.e. without the use of composite samples (e.g., over 24 h) as
426 in the current investigation.
427
428 Ti removal in HØRA is most likely related to association with solids (Fig. 4–5), which are
429 mostly removed during settling and other separation processes. Ti concentrations in biosolids
430 from LARA and HØRA were comparable to those measured in primary sludge (700 ± 200 µg
431 $g^{-1}$) from a WWTP in the US (Kiser et al. 2009). Previously reported Ti concentration in
432 sewage sludge and biosolids ranged from 97 to 4510 mg $kg^{-1}$ (Kim et al. 2012, Westerhoff et
433 al. 2015). Furthermore, we observed agglomerates and aggregates of $TiO_2$ particles reaching
434 500 nm to >1 µm in size (Fig. 6, Fig. S3), which may also settle independently. This is in
435 agreement with previous research reporting a 97% removal of $TiO_2$ NPs in the presence of
436 biosolids, and a 65% removal in the absence of biosolids caused by aggregation and
437 sedimentation (Wang et al. 2012).
438
439 ***4.2. Influx, removal and release of Ag***
440 Influent Ag concentrations (<150–2140 ng $L^{-1}$) were 100–1000 times lower than Ti
441 concentrations in both WWTPs, being generally in good agreement with other findings. A
442 recent study in Sweden reported average total Ag concentrations of 10–2200 ng $L^{-1}$ (490 ± 670
443 ng $L^{-1}$) in the influent of 11 WWTPs (Östman et al. 2017). In a monitoring campaign in several
444 WWTPs in the UK, total Ag concentrations were on average 3310 ng $L^{-1}$, with approximately
445 12 ng $L^{-1}$ (0.36%) being in the colloidal fraction (there defined with size 2–450 nm) (Johnson
446 et al. 2014). In Germany, total Ag influent concentrations ranged from 350 to 760 ng $L^{-1}$, with
447 a peak concentration of 3050 ng $L^{-1}$ in one of the WWTPs (Li et al. 2013). Ag in WWTP

448 influent may also include its sulfidized form, which is known to form during transport in
449 sewers (Kaegi et al., 2013).
450
451 The removal efficiency of Ag in the current study was on average 69–78 %, being 10 % higher
452 in LARA than HØRA. Reduced removal efficiency was observed during the first sampling day
453 at HØRA (47%), most likely resulting from the influent Ag concentration peak during
454 Thursday-Friday evening (Fig. 8c; Fig. S2). Due to the relatively short WWTP residence time,
455 this peak propagated to the effluent, resulting in an increased effluent Ag concentration of 0.9
456 µg $L^{-1}$. Higher removal efficiencies (>93%) compared to the current study have been reported
457 elsewhere (Li et al. 2012, Johnson et al. 2014, Östman et al. 2017). Similarly to Ti, all the
458 WWTPs investigated employed secondary and/or tertiary treatment, which may have led to
459 increased Ag removal.
460
461 ***4.3. Characterization of Ti and Ag***
462 Characterization of Ti and Ag was performed through size-based fractionation by means of
463 sequential filtration and STEM analyses. Detected Ti was strongly associated with wastewater
464 solids, with >99% of influent concentration being measured in the particulate fraction (>0.7
465 µm) in both WWTPs. $TiO_2$ nano- and micro-particles were frequently detected using STEM
466 analysis in both untreated samples and >0.7 µm fraction, with particle size ranging from 50–
467 500 nm up to more than 1 µm. The association of $TiO_2$ to solids is suggested as the main
468 reason for most Ti being in the particulate fraction, supported by a strong correlation between
469 Ti and TSS for both WWTPs (Fig. 4b). Strong association of Ti with suspended solids is
470 consistent with other studies, where 81–96% of the total Ti in wastewater influent was
471 associated with solids >0.7 µm (Kiser et al. 2009).

Most Ag (95–97 %) in wastewater influent was in the particulate fraction (>0.7 µm). However, it was not possible to detect Ag (nano)particles with STEM in influent or effluent samples. This may be due to the low Ag concentrations and the association of both Ag particles and ions to solids, as shown in previous studies (Li et al. 2013, Kaegi et al. 2011, Wang et al. 2012, Kiser et al. 2010). Ag NPs were observed in biosolids (Fig. 7b), but it is unclear whether they were related to the presence of Ag in NP form (at low concentrations) in the influent, or whether Ag in dissolved form underwent transformation (e.g., to $Ag_2S$ NPs) during treatment (Kim et al., 2010). Further investigation should therefore elucidate whether Ag released with WWTP effluents occurs in nanoparticulate form, also in consideration of influent-to-effluent load propagation in Norwegian WWTPs with primary treatment.

### *4.4. Release patterns and sources of discharge*

Diurnal Ti concentrations at both WWTPs were characterized by M and/or E peaks with a significant decrease during the night period. This indicates that Ti discharge follows household discharges, and is in agreement with previous observations for similar catchments and conditions (Becouze-Lareure et al. 2016). Conversely, Ag concentrations in HØRA influent exhibited a significant increase during Thursday-Friday evening periods, resulting from short-term discharge to the sewer system. Ag discharges to HØRA appear to be influenced by one point source, possibly related to industrial activities. Similar observations in WWTP influent have been made for Ti, where industrial contribution to increased Ti loading was postulated (Kiser et al. 2009).

Correlation analysis was used to elucidate sources of discharge by assessing co-occurrence of Ti and Ag with other parameters routinely measured in untreated wastewater. This

496 methodology has been previously applied to identify sources and pathways of pharmaceutical
497 discharge (Plósz et al. 2010, Snip et al. 2016). The rather strong correlation of Ti with TSS
498 suggests either a strong binding to solids, which may have occurred to some extent during in-
499 sewer transport, or a common source. Interestingly, comparable amounts of Ti were quantified
500 per mass of TSS in both WWTPs (0.47–0.49 µg Ti $mgTSS^{-1}$) over the duration of the sampling
501 campaign, suggesting rather similar binding potential to solids in raw sewage.
502
503 Despite the consistent association with wastewater solids, Ag exhibited a rather good
504 correlation with P (except for recurring peak values). The co-occurrence of Ag and P may
505 therefore suggest their combined discharge in wastewater. Phosphorus (mostly in phosphate
506 form) is present in commercial products such as detergents, despite regulatory efforts to limit
507 its use. Accordingly, a number of studies have reported on the release of Ag from textiles
508 during washing with (Geranio et al. 2009, Lorenz et al. 2012) or without (Mitrano et al. 2014,
509 Lombi et al. 2014) P-containing detergents. Furthermore, silver phosphate was identified in
510 unwashed textiles and its formation was observed after washing with P-containing detergent
511 (Lombi et al. 2014). Ag release was also shown to occur from commercial washing machines
512 (Farkas et al. 2011) during laundry cycles. Considering the permissible phosphate content in
513 dishwasher detergents (as of October 2016) in Norway, another potential source of Ag may be
514 dishwashing. Although food containers have been shown to contain and release Ag in
515 nanoparticulate form (Mackevica et al. 2016), no conclusive evidence exists on the release as a
516 result of dishwashing. Furthermore, phosphate is widely used in commercial toothpaste, while
517 Ag has been quantified in both toothpaste (Benn et al. 2010) and toothbrushes (Mackevica et
518 al. 2017). Observations from the current study suggest release of Ag from consumer products

519 through washing and personal care procedures is the main source of *background* emissions to
520 WWTPs (i.e. without considering temporary industrial discharges).
521
522 The information obtained on diurnal patterns and co-occurrence with wastewater pollutants
523 was used to predict Ti and Ag occurrence profiles in WWTP influents. Whilst influent
524 generator models have been developed and calibrated for conventional pollutants (Flores-
525 Alsina et al. 2014) and organic micropollutants (Snip et al. 2016), this study represents a first
526 application to metals. Per capita discharge of Ti in the two catchments was estimated to be 42–
527 45 mg $cap^{-1}$ $d^{-1}$, in agreement with previous estimations (Kiser et al. 2009). The estimated Ag
528 load from a point source in HØRA catchment was 14–22 g $d^{-1}$, up to >70% of total influent
529 load during Thursday evening periods. These estimations are in good agreement with
530 calculated emissions from a single laundry facility in a Swiss WWTP catchment (Kaegi et al.
531 2015). For compounds (such as Ti, Ag and other nano-metals) of relatively unknown usage
532 volumes, detailed knowledge of major sources of discharge and estimation of residential and
533 point source contributions would be highly beneficial for short- and long-term predictions of
534 release dynamics.
535
536 **5. Conclusions**
537 The current study quantified and characterized Ti and Ag in influent, effluent and biosolids of
538 two Norwegian WWTPs (LARA and HØRA), with specific attention towards NPs. Intra-day
539 variations of Ti and Ag influx patterns were assessed, and potential discharge sources were
540 determined.
541 • Mechanical and physico-chemical treatment is sufficient to remove ≥70% of Ti and Ag,
542 mostly through binding to solids and solid-liquid separation processes (e.g., primary

sedimentation). As certain WWTP flocculants contain high concentrations of Ti, it is necessary to account for this additional influx when calculating accurate mass balances.

- Ti was frequently detected as nano- and micronized particles bound to wastewater solids, with total amounts correlating strongly with TSS concentrations. The absence of detectable Ag NPs in influent and effluents may be a result of their low concentrations, although their occurrence can be hypothesized based on detection in biosolids.
- Influent Ti concentrations followed typical flow and pollutant trends, i.e. significant decrease during night, indicating households as major discharge sources. The significant weekly spike in influent Ag concentration observed for HØRA is indicative of a point source industrial discharge. Background influent Ag levels correlated positively with total phosphorus concentrations, suggesting release from textiles and personal care products as primary discharge sources.
- For the first time, an influent generator model was successfully used for prediction of Ti and Ag profiles in WWTP influent. Model simulations allowed short-term release dynamics of Ti and Ag to be described and loads from households and point sources (industries) to be determined, thus complementing existing fate and emission models for (nano)metals. Model-based approaches can further serve as a means to enforce chemical abatement strategies by identifying and reducing point source emissions.

**Acknowledgments**

This study was supported by the Norwegian Research Council project NanoWASTE (GA: 238972). The authors are particularly grateful to WWTP operators at LARA and HØRA, especially Grete Klippenvåg Støen. Dr Flores-Alsina gratefully acknowledges the financial support of the collaborative international consortium WATERJPI2015 WATINTECH of the

Water Challenges for a Changing World Joint Programming Initiative (project ID 196) and the funds provided by the Danish Council for Independent Research under the project GREENLOGIC (project number: 7017-00175B).

**References**

Becouze-Lareure, C., Dembélé, A., Coquery, M., Cren-Olivé, C., Barillon, B. and Bertrand-Krajewski, J.L. (2016). Source characterisation and loads of metals and pesticides in urban wet weather discharges. Urban Water Journal 13(6), 600-617.

Benn, T.M. and Westerhoff, P. (2008) Nanoparticle Silver Released into Water from Commercially Available Sock Fabrics. Environmental Science & Technology 42(11), 4133-4139.

Benn, T., Cavanagh, B., Hristovski, K., Posner, J.D. and Westerhoff, P. (2010) The Release of Nanosilver from Consumer Products Used in the Home. Journal of Environmental Quality 39(6), 1875-1882.

Bollmann, U.E., Tang, C., Eriksson, E., Jönsson, K., Vollertsen, J. and Bester, K. (2014) Biocides in urban wastewater treatment plant influent at dry and wet weather: Concentrations, mass flows and possible sources. Water Research 60(Supplement C), 64-74.

Contado, C. and Pagnoni, A. (2008) TiO2 in Commercial Sunscreen Lotion: Flow Field-Flow Fractionation and ICP-AES Together for Size Analysis. Analytical Chemistry 80(19), 7594-7608.

589 De Keyser, W., Gevaert, V., Verdonck, F., De Baets, B., Benedetti, L. (2010). An emission
590 time series generator for pollutant release modelling in urban areas. Environmental
591 Modelling & Software 25(4), 554–561.
592 Farkas, J., Peter, H., Christian, P., Gallego Urrea, J.A., Hassellöv, M., Tuoriniemi, J.,
593 Gustafsson, S., Olsson, E., Hylland, K. and Thomas, K.V. (2011) Characterization of the
594 effluent from a nanosilver producing washing machine. Environment International 37(6),
595 1057-1062.
596 Flores-Alsina, X., Saagi, R., Lindblom, E., Thirsing, C., Thornberg, D., Gernaey, K.V. and
597 Jeppsson, U. (2014) Calibration and validation of a phenomenological influent pollutant
598 disturbance scenario generator using full-scale data. Water Research 51(Supplement C),
599 172-185.
600 Geranio, L., Heuberger, M. and Nowack, B. (2009) The Behavior of Silver Nanotextiles during
601 Washing. Environmental Science & Technology 43(21), 8113-8118.
602 Gernaey, K.V., Flores-Alsina, X., Rosen, C., Benedetti, L. and Jeppsson, U. (2011) Dynamic
603 influent pollutant disturbance scenario generation using a phenomenological modelling
604 approach. Environmental Modelling & Software 26(11), 1255-1267.
605 Gottschalk, F., Sonderer, T., Scholz, R.W. and Nowack, B. (2009) Modeled Environmental
606 Concentrations of Engineered Nanomaterials (TiO2, ZnO, Ag, CNT, Fullerenes) for
607 Different Regions. Environmental Science & Technology 43(24), 9216-9222.
608 Johnson, A.C., Jürgens, M.D., Lawlor, A.J., Cisowska, I. and Williams, R.J. (2014) Particulate
609 and colloidal silver in sewage effluent and sludge discharged from British wastewater
610 treatment plants. Chemosphere 112(Supplement C), 49-55.

611 Kaegi, R., Voegelin, A., Sinnet, B., Zuleeg, S., Hagendorfer, H., Burkhardt, M. and Siegrist,
612 H. (2011) Behavior of Metallic Silver Nanoparticles in a Pilot Wastewater Treatment Plant.
613 Environmental Science & Technology 45(9), 3902-3908.
614 Kaegi, R., Voegelin, A., Ort, C., Sinnet, B., Thalmann, B., Krismer, J., Hagendorfer, H.,
615 Elumelu, M. and Mueller, E. (2013) Fate and transformation of silver nanoparticles in urban
616 wastewater systems. Water Research 47(12), 3866-3877.
617 Kaegi, R., Voegelin, A., Sinnet, B., Zuleeg, S., Siegrist, H. and Burkhardt, M. (2015)
618 Transformation of AgCl nanoparticles in a sewer system — A field study. Science of the
619 Total Environment 535(Supplement C), 20-27.
620 Kim, B., Park, C.S., Murayama, M., Hochella, M.F. (2010) Discovery and characterization of
621 silver sulfide nanoparticles in final sewage sludge products. Environmental Science &
622 Technology 44(19), 7509–7514.
623 Kim, B., Murayama, M., Colman, B.P. and Hochella, M.F. (2012) Characterization and
624 environmental implications of nano- and larger TiO2 particles in sewage sludge, and soils
625 amended with sewage sludge. Journal of Environmental Monitoring 14(4), 1128-1136.
626 Kiser, M.A., Westerhoff, P., Benn, T., Wang, Y., Pérez-Rivera, J. and Hristovski, K. (2009)
627 Titanium Nanomaterial Removal and Release from Wastewater Treatment Plants.
628 Environmental Science & Technology 43(17), 6757-6763.
629 Kiser, M.A., Ryu, H., Jang, H., Hristovski, K. and Westerhoff, P. (2010) Biosorption of
630 nanoparticles to heterotrophic wastewater biomass. Water Research 44(14), 4105-4114.
631 Lai, F.Y., Bruno, R., Leung, H.W., Thai, P.K., Ort, C., Carter, S., Thompson, K., Lam, P.K.S.
632 and Mueller, J.F. (2013) Estimating daily and diurnal variations of illicit drug use in Hong
633 Kong: A pilot study of using wastewater analysis in an Asian metropolitan city. Forensic
634 Science International 233(1), 126-132.

635 Li, L., Hartmann, G., Döblinger, M. and Schuster, M. (2013) Quantification of Nanoscale
636 Silver Particles Removal and Release from Municipal Wastewater Treatment Plants in
637 Germany. Environmental Science & Technology 47(13), 7317-7323.
638 Lombi, E., Donner, E., Scheckel, K.G., Sekine, R., Lorenz, C., Goetz, N.V. and Nowack, B.
639 (2014) Silver speciation and release in commercial antimicrobial textiles as influenced by
640 washing. Chemosphere 111(Supplement C), 352-358.
641 Lorenz, C., Windler, L., von Goetz, N., Lehmann, R.P., Schuppler, M., Hungerbühler, K.,
642 Heuberger, M. and Nowack, B. (2012) Characterization of silver release from commercially
643 available functional (nano)textiles. Chemosphere 89(7), 817-824.
644 Mackevica, A., Olsson, M.E. and Hansen, S.F. (2016) Silver nanoparticle release from
645 commercially available plastic food containers into food simulants. Journal of Nanoparticle
646 Research 18(1), 5.
647 Mackevica, A., Olsson, M.E. and Hansen, S.F. (2017) The release of silver nanoparticles from
648 commercial toothbrushes. Journal of Hazardous Materials 322(Part A), 270-275.
649 Mitrano, D.M., Rimmele, E., Wichser, A., Erni, R., Height, M. and Nowack, B. (2014)
650 Presence of Nanoparticles in Wash Water from Conventional Silver and Nano-silver
651 Textiles. ACS Nano 8(7), 7208-7219.
652 Mitrano, D.M., Lombi, E., Dasilva, Y.A.R. and Nowack, B. (2016) Unraveling the Complexity
653 in the Aging of Nanoenhanced Textiles: A Comprehensive Sequential Study on the Effects
654 of Sunlight and Washing on Silver Nanoparticles. Environmental Science & Technology
655 50(11), 5790-5799.
656 Ort, C., Schaffner, C., Giger, W., Gujer, W. (2005). Modelling stochastic load variations in
657 sewer systems. Water Science & Technology 52(5), 113−122.

Peters, R.J.B., van Bemmel, G., Herrera-Rivera, Z., Helsper, H.P.F.G., Marvin, H.J.P., Weigel, S., Tromp, P.C., Oomen, A.G., Rietveld, A.G. and Bouwmeester, H. (2014) Characterization of Titanium Dioxide Nanoparticles in Food Products: Analytical Methods To Define Nanoparticles. Journal of Agricultural and Food Chemistry 62(27), 6285-6293.

Plósz, B.G., Leknes, H., Liltved, H. and Thomas, K.V. (2010) Diurnal variations in the occurrence and the fate of hormones and antibiotics in activated sludge wastewater treatment in Oslo, Norway. Science of the Total Environment 408(8), 1915-1924.

Ramin, P. (2016) Modelling illicit drug fate in sewers for wastewater-based epidemiology. PhD, Technical University of Denmark.

Sabin, L.D., Lim, J.H., Stolzenbach, K.D. and Schiff, K.C. (2005) Contribution of trace metals from atmospheric deposition to stormwater runoff in a small impervious urban catchment. Water Research 39(16), 3929-3937.

Shafer, M.M., Overdier, J.T. and Armstong, D.E. (1998). Removal, partitioning, and fate of silver and other metals in wastewater treatment plants and effluent-receiving streams. Environmental Toxicology and Chemistry 17(4), 630-641.

Snip, L.J.P., Flores-Alsina, X., Aymerich, I., Rodríguez-Mozaz, S., Barceló, D., Plósz, B.G., Corominas, L., Rodriguez-Roda, I., Jeppsson, U. and Gernaey, K.V. (2016) Generation of synthetic influent data to perform (micro)pollutant wastewater treatment modelling studies. Science of the Total Environment 569(Supplement C), 278-290.

Sun, T.Y., Bornhöft, N.A., Hungerbühler, K. and Nowack, B. (2016) Dynamic Probabilistic Modeling of Environmental Emissions of Engineered Nanomaterials. Environmental Science & Technology 50(9), 4701-4711.

680 Vogelsang, C., Grung, M., Jantsch, T.G., Tollefsen, K.E. and Liltved, H. (2006) Occurrence
681 and removal of selected organic micropollutants at mechanical, chemical and advanced
682 wastewater treatment plants in Norway. Water Research 40(19), 3559-3570.
683 Wang, Y., Westerhoff, P. and Hristovski, K.D. (2012) Fate and biological effects of silver,
684 titanium dioxide, and C60 (fullerene) nanomaterials during simulated wastewater treatment
685 processes. Journal of Hazardous Materials 201–202(0), 16-22.
686 Weir, A., Westerhoff, P., Fabricius, L., Hristovski, K. and von Goetz, N. (2012) Titanium
687 Dioxide Nanoparticles in Food and Personal Care Products. Environmental Science &
688 Technology 46(4), 2242-2250.
689 Westerhoff, P., Song, G., Hristovski, K. and Kiser, M.A. (2011) Occurrence and removal of
690 titanium at full scale wastewater treatment plants: implications for TiO2 nanomaterials.
691 Journal of Environmental Monitoring 13(5), 1195-1203.
692 Westerhoff, P., Lee, S., Yang, Y., Gordon, G.W., Hristovski, K., Halden, R.U. and Herckes, P.
693 (2015) Characterization, Recovery Opportunities, and Valuation of Metals in Municipal
694 Sludges from U.S. Wastewater Treatment Plants Nationwide. Environmental Science &
695 Technology 49(16), 9479-9488.
696 Östman, M., Lindberg, R.H., Fick, J., Björn, E. and Tysklind, M. (2017) Screening of biocides,
697 metals and antibiotics in Swedish sewage sludge and wastewater. Water Research
698 115(Supplement C), 318-328.

699 **Figures**

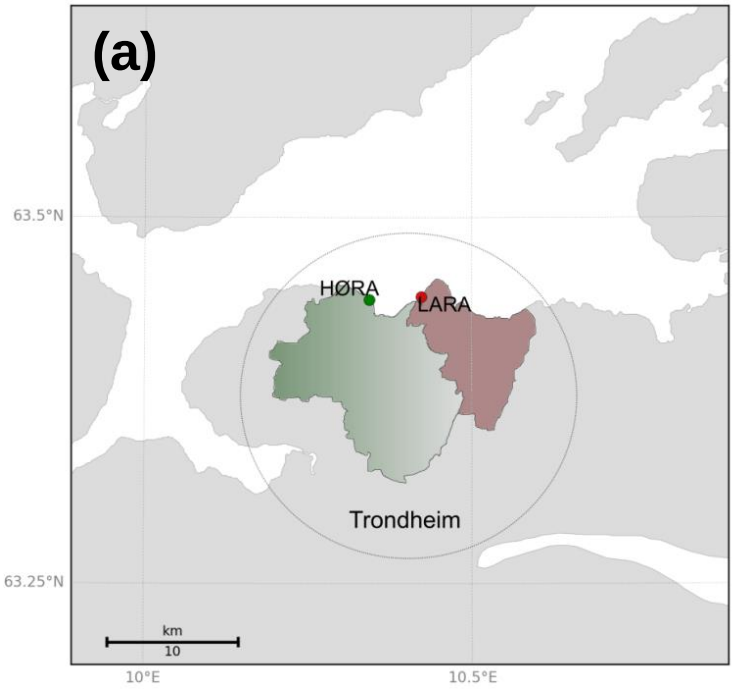


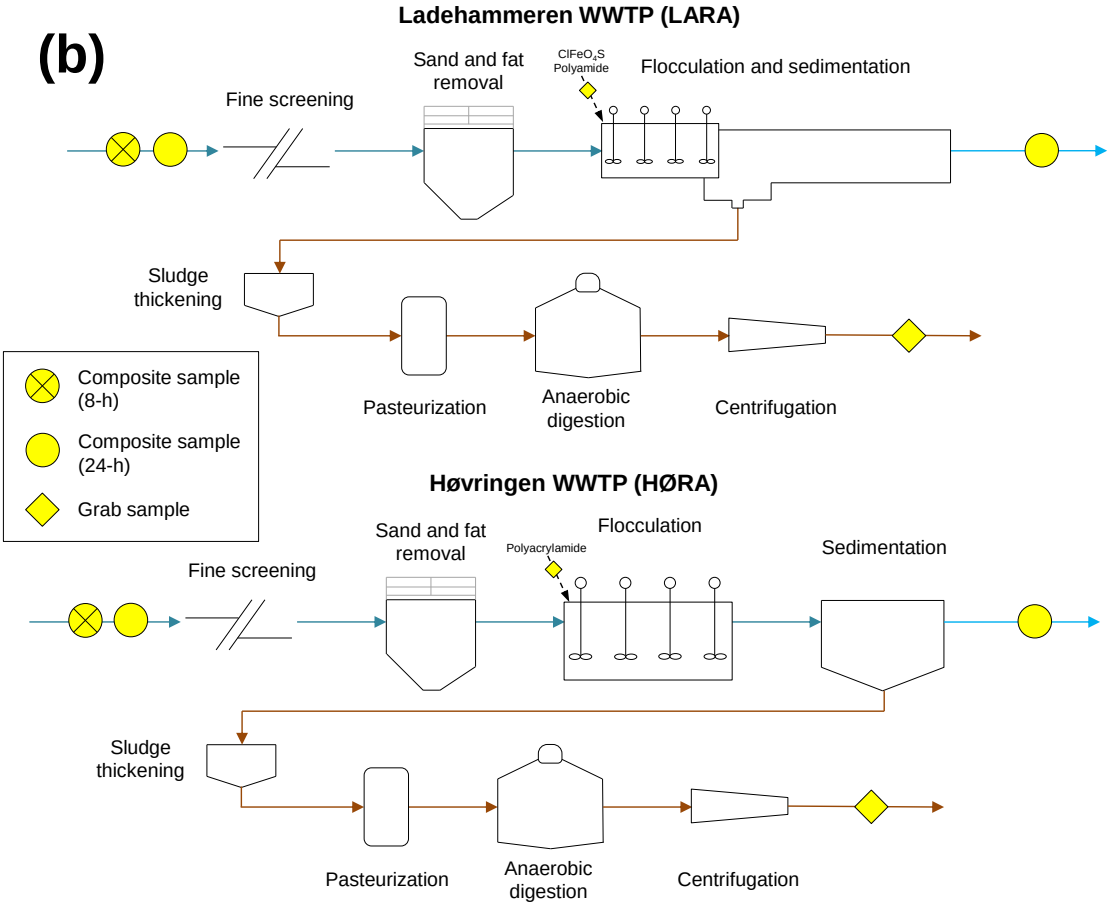


700

**Figure 1.** (a) Map of Trondheim, with location of LARA and HØRA WWTPs and area of the served catchments (19.3 and 48.3 $km^2$ respectively). (b) Flow-sheet diagram of LARA and HØRA. Yellow symbols denote the three sampling points and the respective sampling modes, i.e. untreated influent (8-h flow-proportional composite samples, 24-h volume- or flow-proportional samples), final effluent (24-h volume-proportional composite samples) and treated sludge (grab samples).

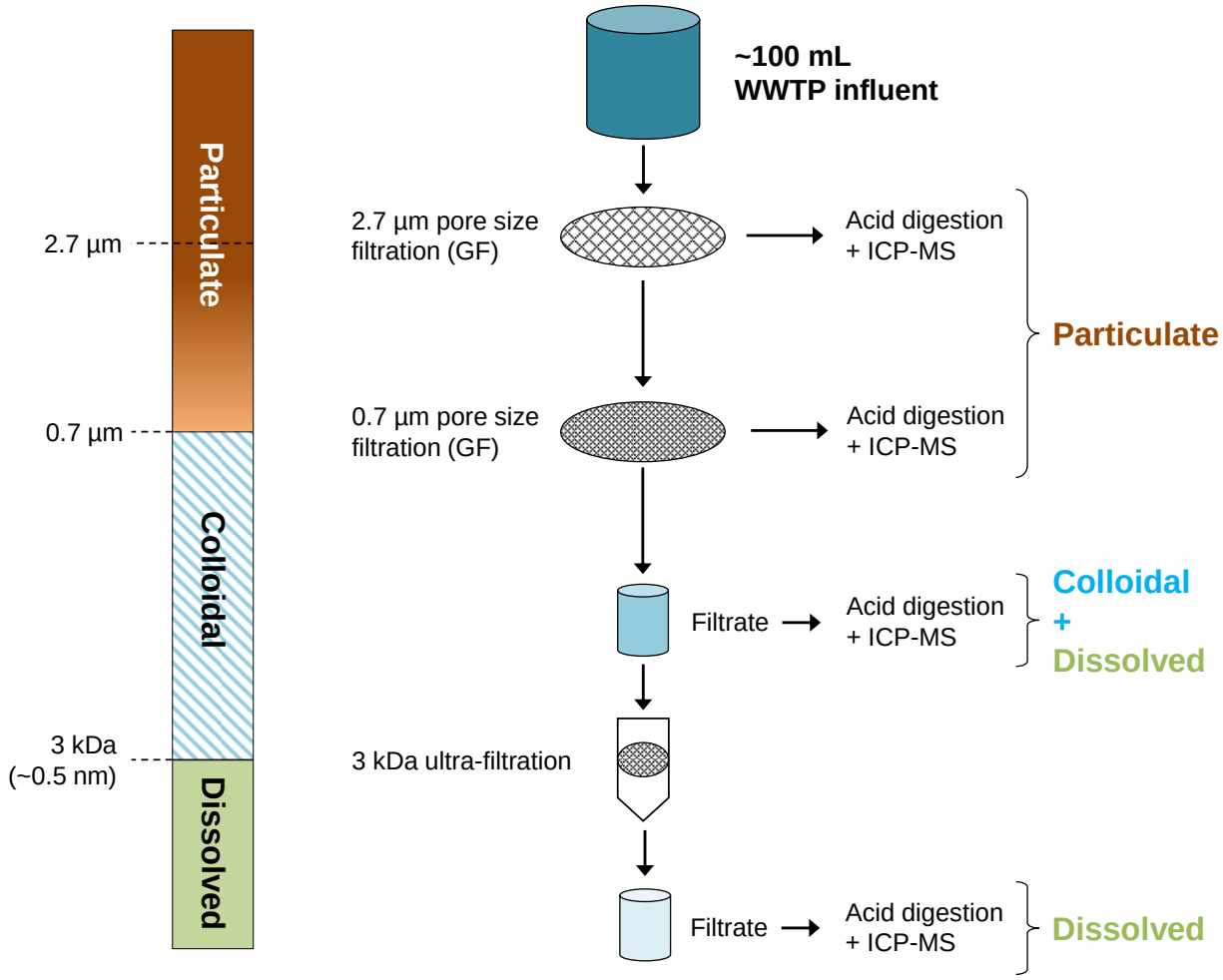


**Figure 2.** Fractionation procedure used to separate and characterize Ti and Ag as particulate, colloidal and dissolved (ionic) fractions.

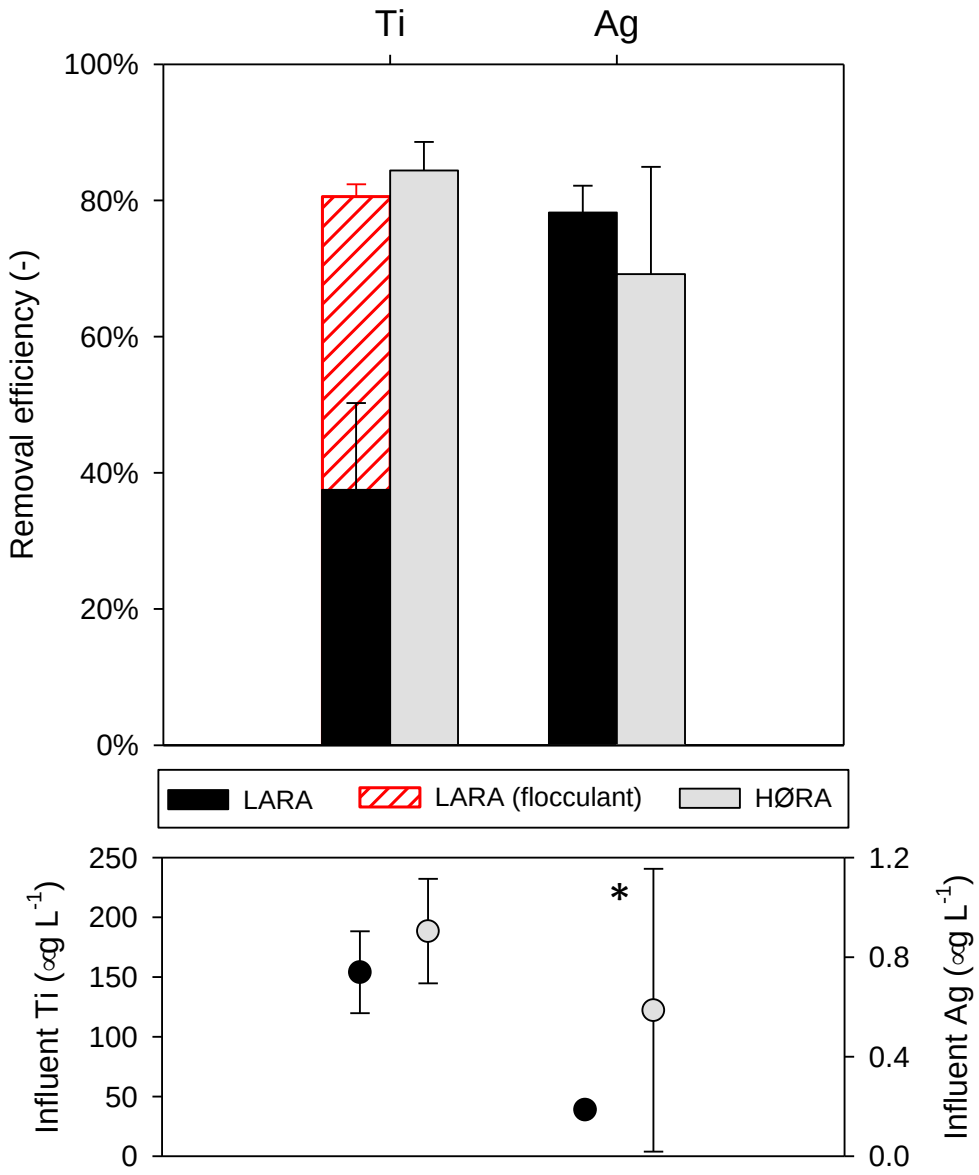


711

712 **Figure 3.** Removal efficiencies and influent concentrations (mean and standard deviation) of
713 Ti and Ag in LARA (*n*=6) and HØRA (*n*=5). For LARA, removal efficiency of Ti was also
714 calculated by accounting for influent Ti load with flocculant. Reported influent Ti and Ag
715 concentrations were measured in 24-h composite influent samples. The asterisk (*) denotes
716 significant differences ($p<0.05$) between the two WWTPs.

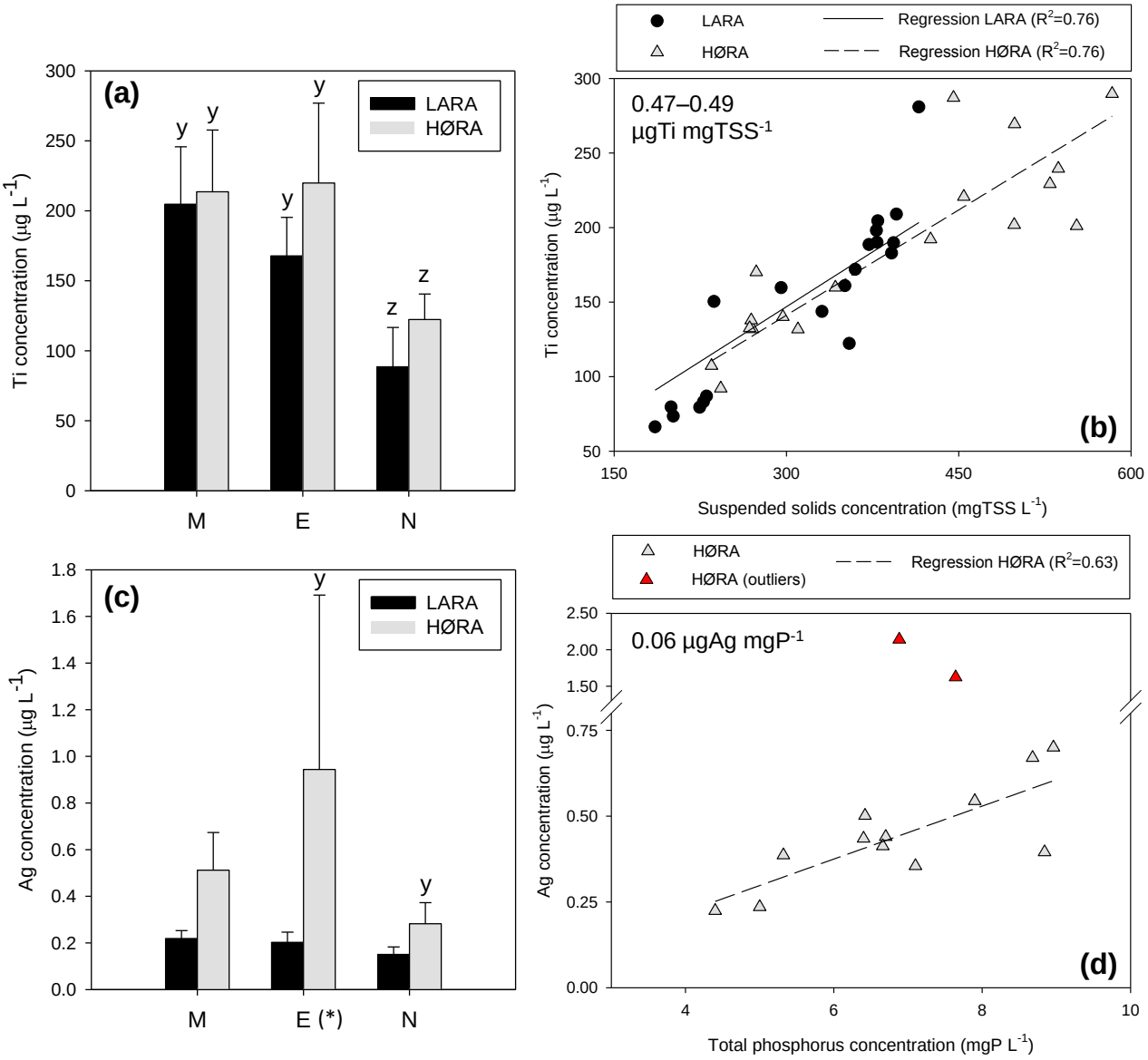


**Figure 4.** Diurnal variations in the occurrence of total Ti (a–b) and Ag (c–d) in LARA and HØRA WWTP influents during the 7-day sampling campaign. Mean total Ti (a) and Ag (c) concentrations are shown for morning (M), evening (E) and night (N) 8 h intervals. Correlations are shown between influent Ti and TSS concentrations in LARA and HØRA (b) and between influent Ag and total phosphorus concentrations in HØRA (d). For Ag, red symbols denote outliers (concentrations higher than 1.5 µg $L^{-1}$). Different letters in (a) and (c) indicate that, for the same WWTP, the influent concentration in one 8-h period is significantly ($p<0.05$) different from one other 8-h period (y) or both other 8-h periods (z). Single asterisks

726 in (a) and (c) denote significant differences ($p<0.05$) between the two WWTPs for the same 8-
727 h period.

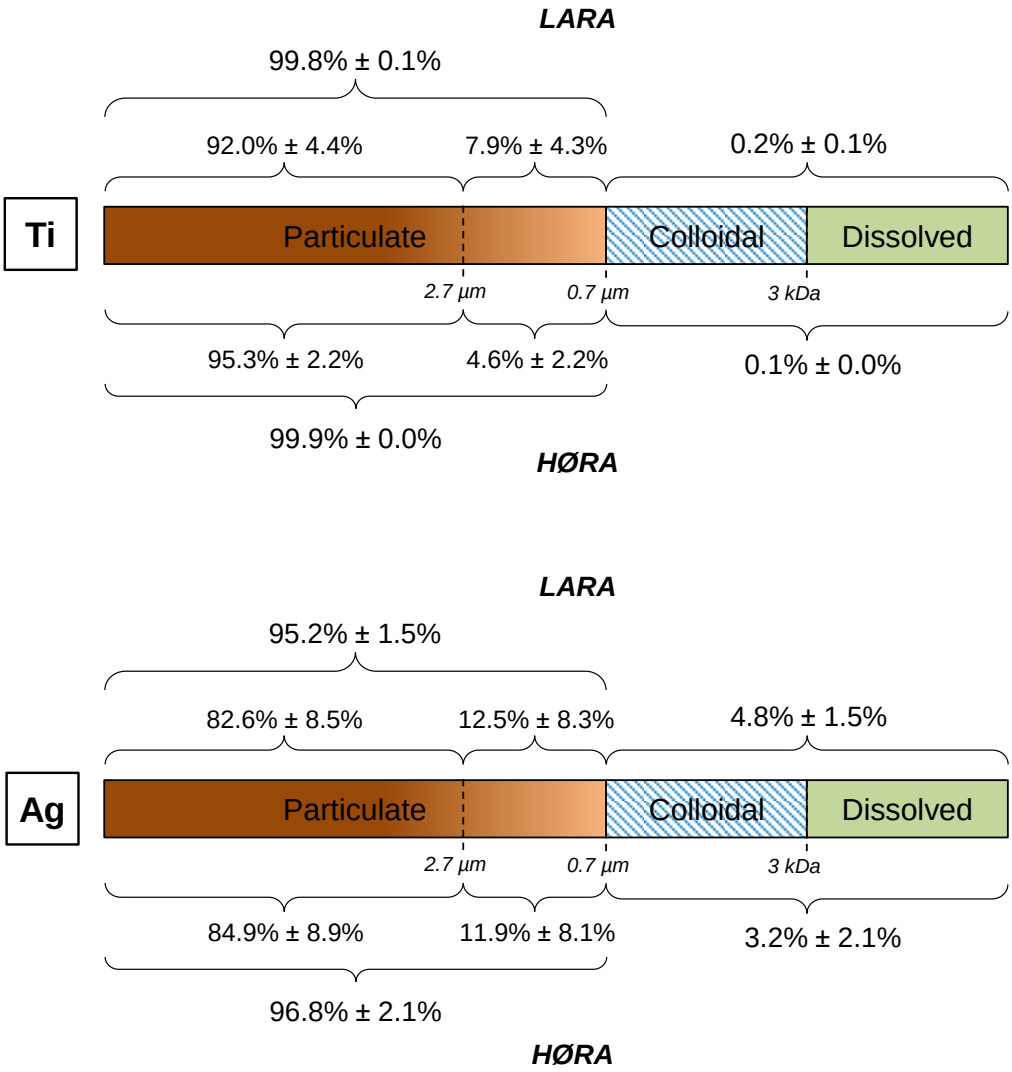


728

729 **Figure 5.** Fractionation of Ti and Ag in WWTP influents, and percentage composition of each
730 fraction (LARA: Ti: *n*=20, Ag: *n*=14; HØRA: Ti: *n*=18, Ag: *n*=14). For clarity, the bar lengths
731 of the individual fractions for Ti and Ag are not presented proportionally.

732

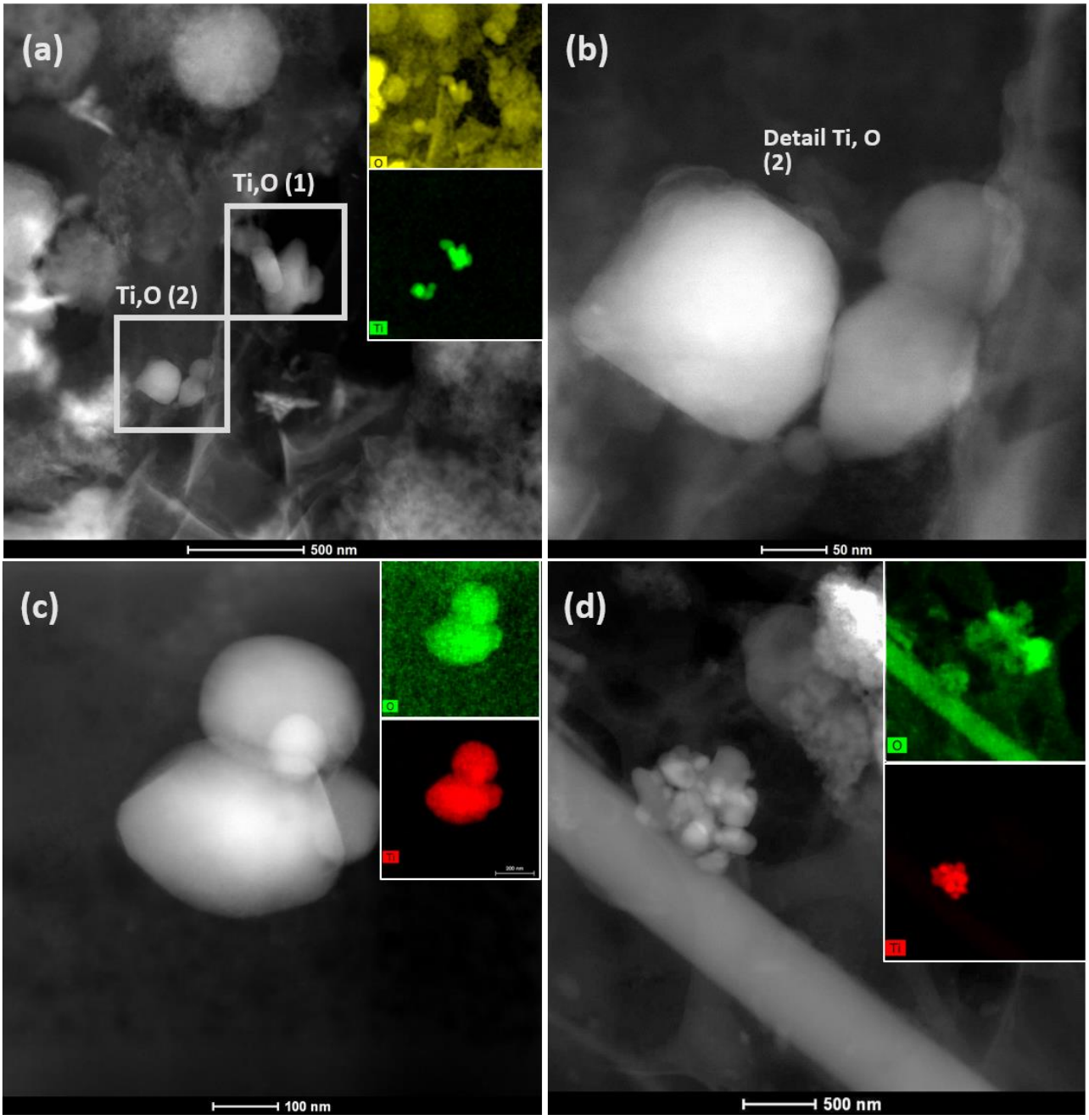


**Figure 6.** STEM images and elemental analysis (EDS, insert images) of $TiO_2$ particles in wastewater samples. (a) $TiO_2$ particles (O is displayed in yellow; Ti in green) in influent wastewater from LARA. Particles are associated with wastewater solids, with details shown in (b). Small (c) and large (d) agglomerates of $TiO_2$ particles (O shown in green, Ti in red) found in the particulate fraction (influent, evening sample E) from HØRA.

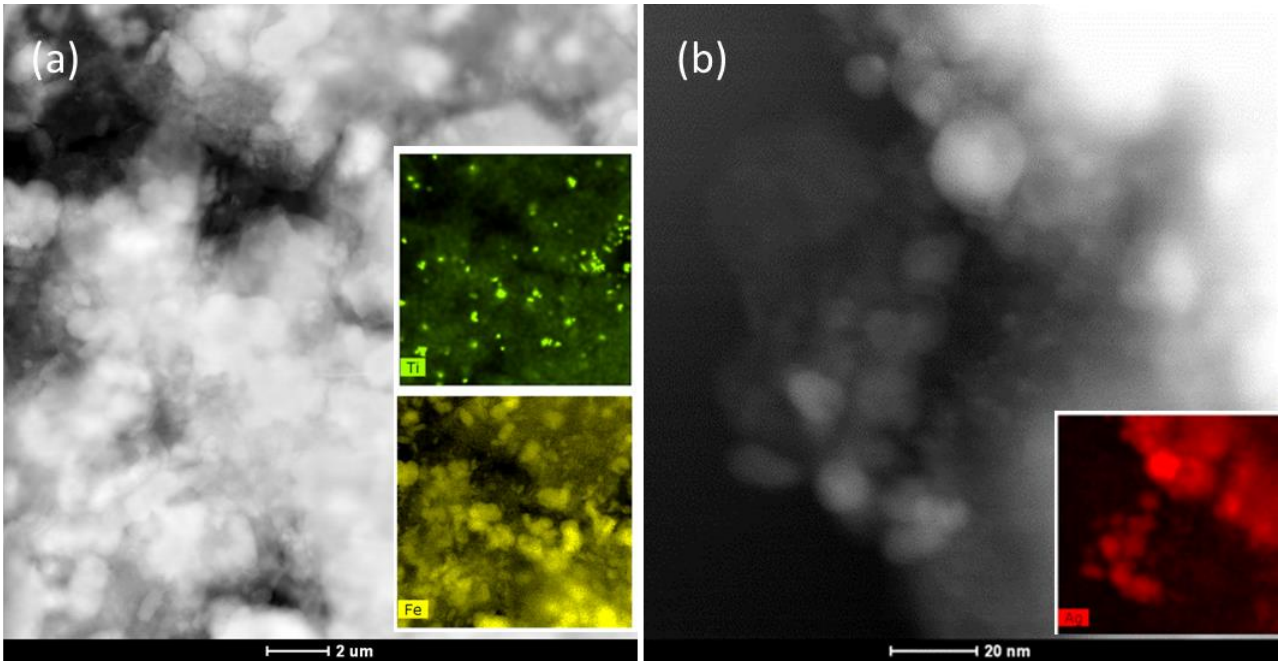


739

740 **Figure 7**. STEM images and elemental analysis (EDS; insert images) of biosolids samples

741 (sludge) from LARA. (a) Ti particles (green) associated with Fe (yellow) containing material.

742 (b) Ag NPs (Ag displayed in red).

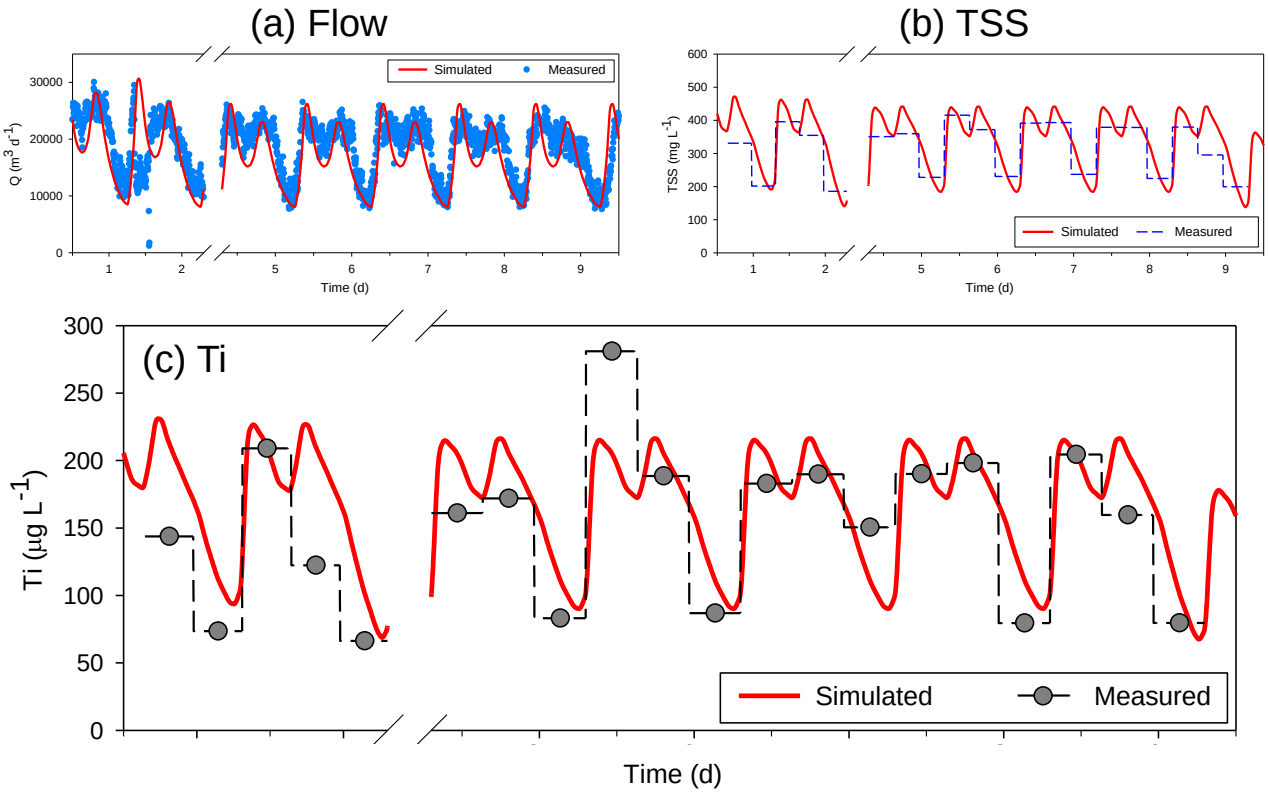


743

744 **Figure 8.** Measured and simulated profiles for (a) influent flow rate, (b) TSS concentration and

745 (c) Ti concentration in LARA during the sampling campaign period.

746

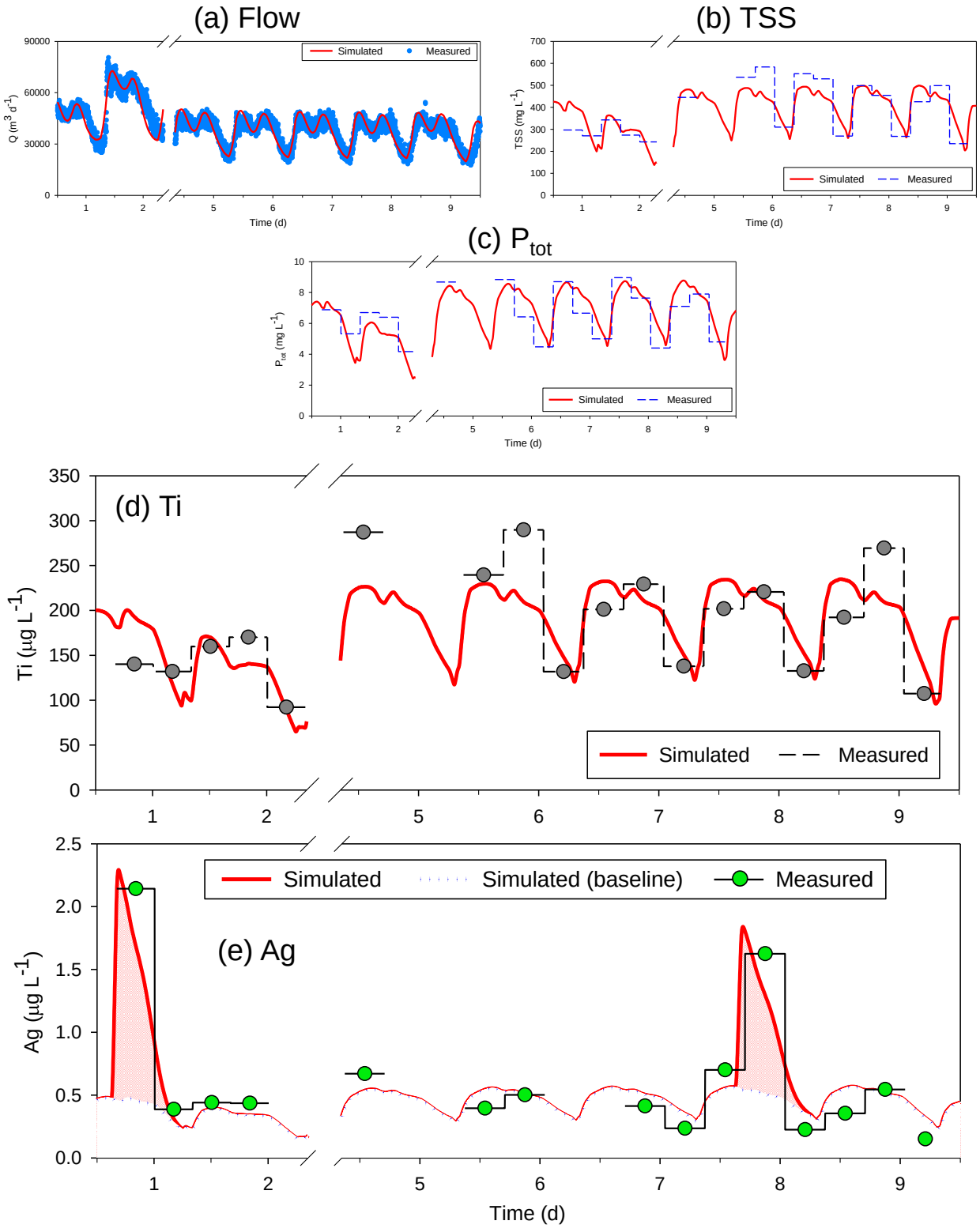


747

748 **Figure 9.** Measured and simulated profiles for (a) influent flow rate, (b–c) TSS and $P_{tot}$

749 concentrations, (d–e) Ti and Ag concentrations in HØRA during the sampling campaign.

750 Model simulations of peak Ag concentrations in influent (e) are shown in red.